Lagrangian Flow Skeletons Captured in the Wake of a Swimming Nematode *C. elegans* Using an Immersed Boundary Fluid-Structure Interaction Approach

Arash Taheri

Abstract—In this paper, Lagrangian coherent structure (LCS) concept is applied to wake flows generated in the up/down-stream of a swimming nematode *C. elegans* in an intermediate *Re* number range, i.e., 250-1200. It materializes Lagrangian hidden structures depicting flow transport barriers. To pursue the goals, nematode swimming in a quiescent fluid flow environment is numerically simulated by a two-way fluid-structure interaction (FSI) approach with the aid of immersed boundary method (IBM). In this regard, incompressible Navier-Stokes equations, fully-coupled with Lagrangian deformation equations for the immersed body, are solved using *IB2d* code. For all simulations, nematode's body is modeled with a parametrized spring-fiber built-in case available in the computational code. Reverse von-Kármán vortex street formation and vortex shedding characteristics are studied and discussed in details via LCS approach, including grid resolution, integration time and Reynolds number effects. Results unveil presence of different flow regions with distinct fluid particle fates in the swimming animal's wake and formation of so-called 'mushroom-shaped' structures in attracting LCS identities.

Keywords—Lagrangian coherent structure, nematode swimming, fluid-structure interaction, immersed boundary method, bionics.

I. INTRODUCTION

FORMATION and ejection of vortices in the wake of a swimming animal is a common bio-propulsion mechanism in nature [1]. This principle can be applied to all anguilliform [2], carangiform [3], ostraciiform and also thunniform [4] swimmers. In general, generation and control of ejected vortices are majorly governed by the animal's body deflection dynamics [5]. As an example, a jellyfish produces stopping/ starting vortices by a cyclic time-dependent body deflection to propel itself in the fluid flow environment [6]. Any factor that can interfere with the process of vortex generation has a capability to affect the propulsion performance. For instance, nonlinear deformations of tentacles interacting with the bell dynamics in the jellyfish swimming can disturb its vortex generation processes and ultimately affect the swimming speed [7]. In addition, eidonomy (i.e., external morphology/ geometry) of oscillating and also non-oscillating sections of the animal's body can basically modify characteristics of the ejected vortices [8] and swimming hydrodynamics in general (e.g., separation zones, drag and lift force generation, etc.) [9]-[11]. As an example, presence of the dorsal ridges on a whale shark's body uniformize energy content of the wake's vortical structures ejected by cyclic oscillations of the tail or more precisely, 'caudal peduncle' [8].

Nematodes, e.g., *C. elegans*, are bilaterally symmetrical round-worms that possess tubular body-shape and a simple circular cross-section (Fig. 1 (a)) [12], with possible extra eidonomic features like rings, ridges and bristles on the body surface in general [13]. However, these extra features are neglected for *C. elegans* as in our computations here. As an anguilliform swimmer, a nematode basically propels itself by consecutive deflections of its body with a cyclic changing of body curvature (concavity/convexity sign) in the fluid flow environment [14], in a low [15] to an intermediate *Re* number. Experiments [16], [17] and numerical simulations [18] show that anguilliform swimmers efficiently change characteristics of their 'body curvature' dynamics (for both escape and steady swimming modes) to overcome necessities of life in their natural habitat. For example, nematode, *C. elegans*, hires a fast and large stroke to swim in a highly viscous medium (e.g., in the shear thinning regime of a non-Newtonian colloidal suspension) [17] and a lamprey, *Petromyzon marinus*, hires a high amplitude body bend to accelerate in escape swimming modes [16]. On the other hand, the steady swimming mode, as considered in the present computation, is characterized by shallower body bend (curvature), hence with different body stiffness present in the acceleration mode [18].

In general, swimming of an animal with a deformable body in a flow field can be simulated by an FSI approach. In this regard, IBM is an interesting technique, which numerically solves Navier-Stokes equations coupled with the equations of the flexible immersed boundary in a single two-way framework [19]. IBM has been extensively used for a broad range of bio-fluid FSI applications such as, heart valves, fish and plankton swimming [2], [20]. In the present paper, quasi-steady and start-up phases of the locomotion for a swimming nematode in a quiescent fluid flow environment at different Re are simulated by the aid of an open-source fully-coupled FSI-IBM code, namely *IB2d* [21]-[22]. Ejections of vortices in the downstream wake of *C. elegans*, i.e., formation of the reverse von-Kármán vortex street, along with upstream flow structures are studied here in details using LCS concept. With the aid of the latter technique, convective fluid flow barriers as hidden attracting and repelling flow structures are numerically identified in the computational domain [23]. In the upcoming sections, details are presented.

Arash Taheri, Ph.D., Mech. Eng., Division of Applied Computational Fluid Dynamics, Biomimetic and Bionic Design Group, Tehran, Iran (e-mail: taha.bionics @gmail.com).

II. NUMERICAL METHODOLOGY

Generated wakes in *C. elegans* swimming are simulated at different Reynolds number using a fully-coupled FSI-IBM code, i.e. *IB2d*, developed by Battista et al., currently director of Bio-Inspired Computation and Experiments (BICEP) lab in the Mathematics and Statistics Department of the college of New Jersey (TCNJ) [21], [22], [24]. *IB2D* basically adopts a blending Eulerian-Lagrangian strategy based on Peskin's IBM approach [19]. In fact, 'fluid solver' part of the code uses a Eulerian approach, while solid (immersed boundary) solver utilizes a Lagrangian approach. Governing equations of the incompressible flow field, i.e., incompressible Navier-Stokes equations, can be formulated as [21], [22], [24]:

$$\rho\left(\frac{\partial u_i(x,t)}{\partial t} + u_j(x,t)\cdot\frac{\partial u_i(x,t)}{\partial x_j}\right) = -\frac{\partial p(x,t)}{\partial x_i} + \mu\frac{\partial^2 u_i(x,t)}{\partial x_j\partial x_j} + f_i(x,t)$$

(1)

$$\frac{\partial u_i(x,t)}{\partial x_i} = 0$$

(2)

where ρ, μ and $f_i(x,t)$ are fluid density, dynamic viscosity and a FSI term, respectively. The latter term is evaluated by a modeling of the fiber component in the aforementioned code, as [21], [22]:

$$f_i(x,t) = \int F_i(\xi,t)\,\delta(x - X(\xi,t))\,d\xi$$

(3)

where δ is a delta function. *X* is a material point defined by a Lagrangian parameter ξ on the immersed boundary curve. In addition, different fiber models with different force density functions can be selected in *IB2d* code, including: Hookean, non-Hookean and torsional springs, target points, mass points, porosity and muscle-fluid-structure models [22]. For *C. elegans* swimming, the immersed boundary is made of Hookean springs; in this case, $F_i(\xi,t)$ at a point denoted as *k* can be evaluated as:

$$F_i(\xi,t) = -\frac{\partial E_{spring}}{\partial X_k^i} = -\frac{\partial}{\partial X_k^i}\left[\frac{1}{2}k_{spring}\left(\left\|X_{spring}^k\right\| - L_R^k\right)^2\right]$$

(4)

where E_{spring} and k_{spring} are elastic deformation energy of the immersed boundary and spring stiffness, respectively while X_{spring}^k and L_R^k are compressed/stretched and initial lengths of the springs, respectively. To apply no-slip boundary condition in *IB2D* code, velocity at the immersed boundary points is set as local fluid flow velocity [21], [22]. The code also applies periodic conditions on all boundaries of the computational domain [22]. *IB2D* code has been widely used for different FSI applications so far, such as: flexible beam [22], jellyfish swimming with/without tentacles [6], [7], elastic tube [21], falling sphere in pulsatile flow [22] and idealized anguilliform swimmers [22], [25], [26]. The code was also validated for an insect wing moving laterally/transversally in the flow field, via a comparison to the experimental PIV data [22].

III. GEOMETRY, DYNAMICS AND SIMULATION SETTINGS

Geometry of *C. elegans* can be approximated by a linear section followed by a polynomial curve (Fig. 1 (a)). In the present study, the linear section is assumed over about 28% of the body length and the curve part is defined as $y = x^3$ over 72% of the rest of the body [24]. The immersed body structure of the animal is constructed by spring and beam elements with spring constant and beam stiffness equals to $9.5625\times10^9\,N$ and $2.036\times10^{12}\,N$, respectively. Swimming is then performed via continuous change in the 'body curvature' by interpolating of the consecutive up (phase 1) and down (phase 2) bending of the body in a sinusoidal format by spline interpolation as shown in Fig. 1 (b) [24]. Sensitivity analysis of the swimming performance has been performed with respect to Reynolds number and Stroke frequency [25]-[26]. In the present paper for extraction of LCS in the animal's wake, stroke frequency is set as $f \simeq 2$.

Here it is also assumed that *C. elegans* starts swimming in a quiescent fluid flow field and from rest at $t = 0$, far from the physical boundaries. However, as recently shown for an anguilliform swimmer, ground effect is almost negligible on the swimming performance and also on the ejected vortical structures for a gap/distance larger than 4% of the body-length from physical walls [27]. Computational domain size is set as 12×4 m^2 with grid resolution equals to 768×256 in x and y directions, respectively. All simulation runs are performed for 4 s of a physical time, involving 8 full strokes. Time step is set as 2.5×10^{-5} s for all upcoming simulations. Simulation results including velocity vector and vorticity fields are frequently saved every 0.01 seconds for post-processing process. Results are presented in the following sub-sections.
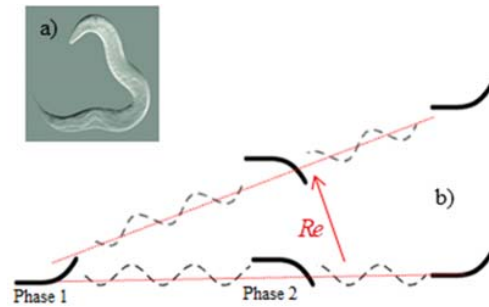

Fig. 1 *C. elegans*: (a) real geometry [12], (b) schematics of swimming pattern in the adopted two-way FSI simulations

IV. NEMATODE SWIMMING

By sequential change of the body curvature, *C. elegans* can effectively swim in the fluid flow environment. Fig. 2 shows variation of Courant–Friedrichs–Lewy (CFL) number in terms of time for the nematode swimming in *Re* range from 250 to 1200. Here *Re* is defined as $\rho u_c L / \mu$, where *L* and μ are the

body length of *C. elegans* and dynamic viscosity, respectively. u_c is the characteristic velocity and defined as $u_c = L.f$, where f is stroke frequency of the body deflection dynamics. As one can see in the figure, with selection of the time step equals to 2.5×10^{-5} s, *CFL* number is low enough during the designed simulations (< 0.011), which keeps simulation runs in the stability margin ($\ll 1$) at all instants of time.
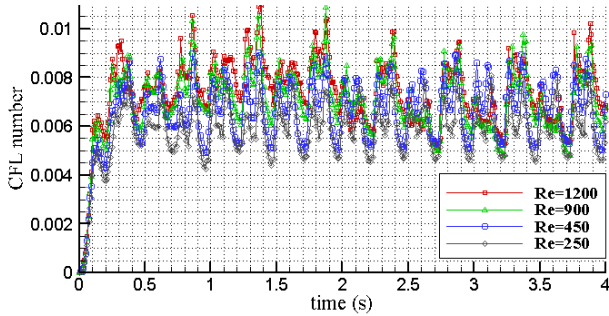

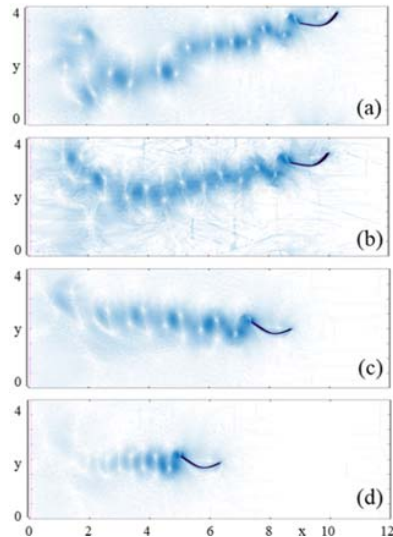Fig. 2 CFL number variations *vs.* time for *C. elegans* swimming simulations at different *Re* number

Fig. 3 Velocity vector field of the nematode swimming in a quiescent flow at different *Re* number equals to: (a) 1200, (b) 900, (c) 450, (d) 250

Fig. 3 shows velocity vector fields generated by *C. elegans* at $t = 4$ s for different *Re*, i.e., after 4 seconds of swimming starting from rest at $t = 0$. As one can see in the figure, by decreasing *Re* to 450 and 250, maximum travel distance of the swimmer (efficiency of the propulsion mechanism) decreases. Signatures of von-Kármán vortex street behind the animal are also visible in the velocity vector fields for all *Re*. In other words, by successive deflection of the body, *C. elegans* repeatedly generates vortices with opposite signs, which are formed, detached from trailing edge of the body and convected downstream, forming von-Kármán vortex street. Fig. 4 depicts pattern of ejected vortices behind the animal at

$t = 4$ s, visualized by z-vorticity (ω_z) thresholding. As shown in Fig. 4, depending on the convexity and concavity of the body's curvature in the bending dynamics, sign of the ejected vortices alternatively changes as time proceeds. In the process, at each stroke a pair of successive negative/positive vortices is generated and then convected downstream sequentially. In addition, it is also obvious in Figs. 3 and 4 that travel trajectory curves of *C. elegans* are obtained by a complicated nonlinear FSI interplay between fluid and solid domains. For *Re* equals to 250 and 450, swimming trajectory is horizontal, while for *Re* equals to 900 and 1200 travel path is inclined and heading upward.
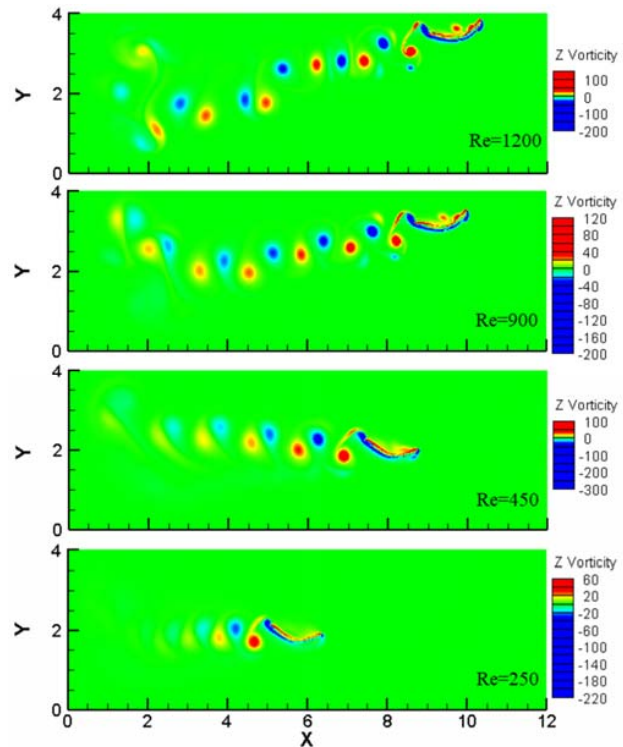

Fig. 4 Ejection of vortices in the wake of the swimming nematode at different *Re* (z-vorticity visualization threshold equals to ± 30)
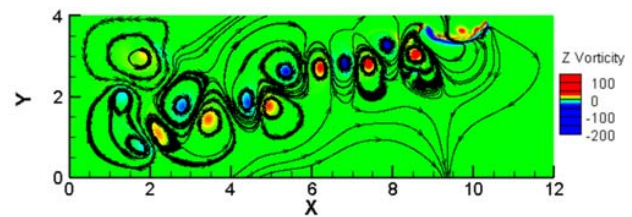

Fig. 5 Streamline pattern in the wake of a swimming nematode superimposed on z-vorticity field at *Re* = 1200

Fig. 5 shows streamline pattern formed behind the animal at $t = 4$ s, at high-intermediate *Re* = 1200. As one can see in the figure, streamlines around a vortex are deflected (detected by z-vorticity, ω_z threshold here) exhibiting a circular pattern, as clarified theoretically by [28]. Interactions of these vortices in

the wake of the swimming animal determine topology of the streamline pattern in general.

V. LCS ANALYSIS

The main goal of this paper is to study Reverse von-Kármán vortex street formation behind a swimming nematode *C. elegans* with the aid of LCS concept, as an effective tool in the dynamical-system field. To detect vortices in a flow field, two kinds of methods exist in general, namely 'Lagrangian' and 'Eulerian' approaches [29]. The latter technique involves some sorts of velocity gradient calculations at local points or pressure value thresholding, such as Q – criterion [30], λ_2 – criterion [31], iso-surface of vorticity (Fig. 4) and iso-surface of pressure, etc. Eulerian technique can detect vortex cores, but fails to capture exact boundary of vortices in the flow field. It also suffers from 'shear contamination', which may bring some errors in the vortex detection process. On the other hand, Lagrangian techniques rely on fluid particle trajectory calculations and artificial seeding [29]. These techniques are able to precisely detect boundary of vortices and also vortex interactions using temporal integration over a period of time. LCS are relatively long-lived identities in the flow field with respect to the time scales of the problem that can basically define convective-transport barriers in the fluid flow system. Hence, multiple zones within the flow field with different ultimate fates can be identified by the structures. To extract LCS in time-dependent flows, one can utilize finite-time Lyapunov exponent (FTLE) measure [23]. Having on hand the FTLE field, LCS can be materialized as ridges exhibiting highest FTLE values in the field. FTLE is obtained by:

$$\xi^{FTLE}_{(X,t_0,T)} = \frac{1}{|T|} \ln \left\| \frac{\delta \Phi^{t_0+T}_{t_0}}{\delta X^{t_0+T}_{t_0}} \right\| \qquad (5)$$

where $\delta \Phi^{t}_{t_0}$ is infinitesimal distance between stretched points over the time interval, namely T [23]. If $T < 0$ (or backward integration fashion), attracting LCS or unstable manifolds are captured; while for $T > 0$ (or forward integration fashion), repelling LCS or stable manifolds are extracted. In this paper, FTLE field is calculated by a mathematical code developed for LCS computations by [32]. In this regard, velocity vector fields computed by *IB2D* in 'vtk' format are saved every 0.01 s for a total time of simulation runs, i.e., 4 s. Then after, these 'vtk' files are read and restructured in a new format readable by the adopted LCS code with the aid of an in-house code here [33].

A. Effects of Grid Resolution on LCS

To study the influence of the grid resolution on the resolved flow structures by LCS technique, a set of grids with three different levels of refinements are considered. Table I shows resolutions (nodes in x and y directions) hired to materialize LCS identities in this sub-section. In this regard, a window, as 4×2 m², around an initial detached structure originated from the trailing edge of the nematode's body after one second of

swimming at $Re = 450$ is considered (Fig. 6). Hence, the data set consists of 100 frames of velocity field saved every 0.01 s, which are fed to the LCS computational code. Fig. 6 depicts effect of grid resolution on the resolved attracting LCS.
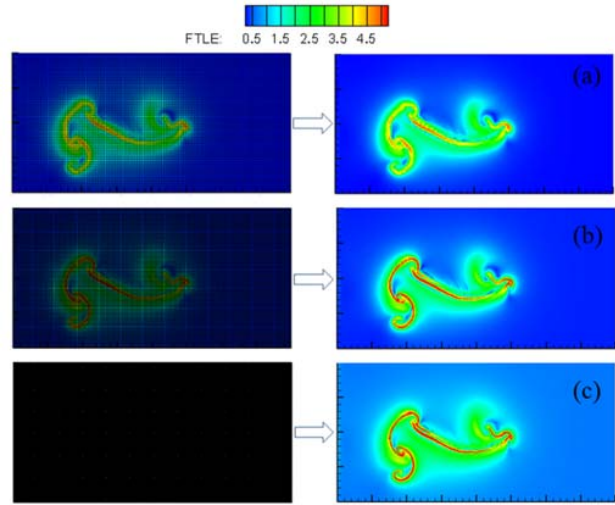

Fig. 6 Grid resolution effects: attracting *LCS* at *Re* = 450: (a) coarse mesh, (b) medium mesh, (c) fine mesh

As one can see in Fig. 6, by increasing the resolution, structures- defined as ridges of the highest FTLE, colored in red (Fig. 6)- emerge more clearly and sharply (Figs. 6 (b) and (c)). As expected a-priori, grid resolution does not affect position of the structures in the flow field. It is also seen in the figure, medium grid exhibits a good compromise between accuracy of the resolved structures and computational cost. In other words, the medium grid resolution here is fined enough (64 nodes/m) to resolve details of LCS for upcoming computations of *C. elegans* swimming with a reasonable computational cost.

TABLE I
GRID SPECIFICATIONS

Mesh	Resolution $n_x \times n_y$
Coarse	128×64
Medium	256×128
Fine	512×256

B. Effects of Integration Time on LCS

In this sub-section, effects of the integration time T on the resolved LCS are considered. In general, 'integration time' affects spatial resolution level of LCS identities [34]. In other words, by increasing the integration time T, more details of LCS are captured. Fig. 7 depicts attracting *LCS* captured at t = 4 s by applying different 'integration time' values as $T = nT_c$, where $T_c = 0.01$ s and the parameter (n) varies in the set defined as {20,50,100,200,400}. In this case, the nematode swims at $Re = 450$ and generates a downstream wake with a repetitive mushroom-like pattern. As one can clearly observe in the figure, by increasing the integration time from (f) to (a),

more '*mushroom-shaped*' sub-structures are captured by the *LCS* computations. Furthermore, more details in attracting LCS emerge by increasing the integration time; the most complete representation is achieved by considering $T = 4$ s.
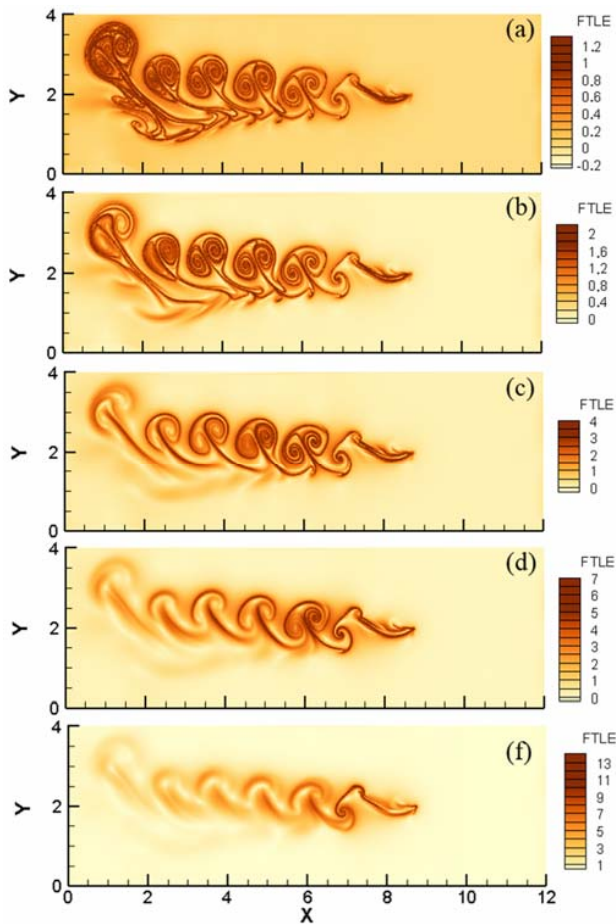

Fig. 7 Integration time effects on attracting LCS with the integration time $T = nT_C$, where $T_C = 0.01s$, for: (a) 400, (b) 200, (c) 100, (d) 50, (f) 20

To understand how a '*mushroom-shaped*' attracting LCS forms in the downstream wake of a swimming *C. elegans*, 'vortex shedding mechanism' involved in the problem should be reviewed in details. In fact, during the time-dependent and repetitive body deflections of the nematode, pairs of vortices with negative ($\omega_z < 0$) and positive ($\omega_z > 0$) vorticity signs are continuously developed, detached from the trailing edge of the animal's body and ultimately ejected into the downstream (marked in the dashed-ovals in Fig. 8 (c). As stated before, these counter-rotating vortices are generated at each full-stroke by a fully-nonlinear time-dependent interplay between fluid and solid media via IBM-FSI method explained earlier.

Fig. 8 (b) shows the mechanism responsible for the formation of the '*mushroom-shaped*' attracting LCS. As mentioned above, vortical system in this case consists of two vortices rotating in the opposite directions. Interaction of these

two vortices forms the external circular boundary of the LCS identity here. In addition, an inclined separatrice is also generated inside the vortical system at the stagnation line, as a direct result of the interaction. As one can see in Fig. 8 (a), an opening exists at the bottom of the continuous circular LCS boundary of the vortical system, which means presence of a fluid transport into or out of this circular LCS boarder over time. Similar phenomenon has been observed by Lipinski et al. about formation of separation bubble on an airfoil, which exhibits penetration of mass into or out of the bubble [34]. The inclined separatrice is also extended more, due to the vortex interactions to join a base semi-straight line (here a semi-horizontal line at $Re = 450$), as shown in Fig. 8 (a).
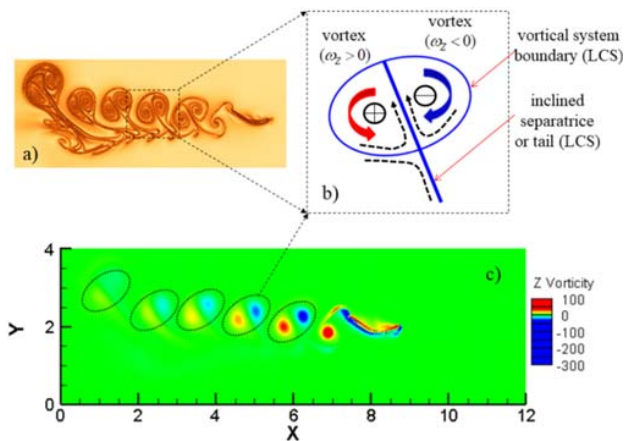

Fig. 8 Formation of '*Mushroom-shaped*' structures at $Re = 450$: (a) attracting LCS, (b) mechanism schematics, (c) ejected vortices

C. Effects of Reynolds Number on LCS

As can be guessed apriori, dynamics of the problem and also 'propulsive reverse von-Kármán wake' behind the animal are substantially affected by changing Re. To study effects of this parameter on the transport barrier structures, Figs. 9 and 10 are considered for attracting LCS at t = 4 s and repelling LCS at t = 0 s, respectively. In the LCS computations, 400 frames with 0.01 time interval have been used. Then with 200 frames, at an intermediate time i.e., t = 2 s, FTLE is obtained; Figs. 11 and 12 are used to extract attracting and repelling LCS, respectively. In these figures, instantaneous position of *C. elegans* has been marked by a vertical 'red' vector.

Fig. 9 depicts effects of Re on the attracting LCS. These structures are material lines (2D) or surfaces (3D) in the flow field that fluid particles close to these structures on its both sides, approach to these structures, as time proceeds. As one can see in the figure, by increasing Re more complicated pattern is obtained by shape deformation and also mixing of LCS. In addition, by increasing Re, swimming performance, i.e., distance travelled by the self-propelled swimmer per time unit, increases up to a certain level ($Re = 900$) and then stays relatively constant. It is also clear that lower than $Re = 450$, swimming performance dramatically decreases and attracting LCS becomes highly tangled. For Re equals to 250 and 450, FSI simulations exhibits a relatively horizontal swimming path

and LCS identities positioned horizontally, while for higher *Re* numbers, i.e., 900 and 1200, LCS are getting more tilted, pointing upward. In addition, width of the portion affected by the swimmer in the downstream flow, i.e. $A_w^b(x)$, grows while moving in x^- direction for all *Re* numbers.
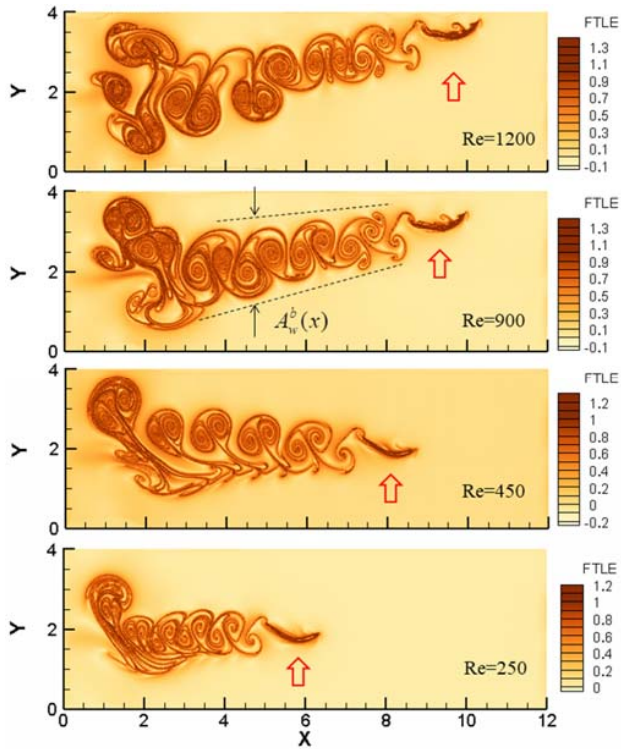

Fig. 9 Attracting LCS (unstable manifolds) via backward LCS computations at $t = 4\,s$, at different Reynolds number

Fig. 10 shows upstream repelling LCS identities generated ahead of a swimming nematode *C. elegans* at t = 0 s, considering integration time as $T = 4$ s. As one can see in the figure, not only prominent propulsive downstream structures or attracting LCS (Fig. 9), are produced by the adopted two-way FSI simulations of the self-propelled animal, but also noticeable upstream repelling LCS identities are produced ahead of the animal (Fig. 10). Similar observation about the 'upstream' repelling LCS has been made in the literature in a one-way simulation (without solid domain solver, i.e., not fully-coupled FSI) for an oscillating flexible plate with applying prescribed kinematics [35]. Upstream repelling LCS identities are also present in a self-propelled jellyfish swimming, generated with the two-way IBM-FSI strategy [6]. As one can see in Fig. 10, repelling LCS map at all *Re* numbers composes of an oscillatory centerline curve with semi-sinusoidal variation shape and successive closed arcs attached to the curve, which generate multiple flow zones with separate ultimate fates in the upstream region. At *Re* = 250 and 450, this so-called 'backbone' curve is almost horizontal, but for *Re* = 900 and 1200 this curve is tilted upward. Width of the repelling structures, i.e., $A_w^f(x)$, clearly declines while

moving in x^+ direction for *Re* = 900 and 1200. Presence of these upstream structures determines which potion of the upstream flow field is affected by the animal swimming over the total time period of swimming or in other words, interacts with the animal. These upstream effects generated by a self-propelled swimmer can basically modify inflow conditions and contribute to its self-propulsion and hence locomotive dynamics [35].
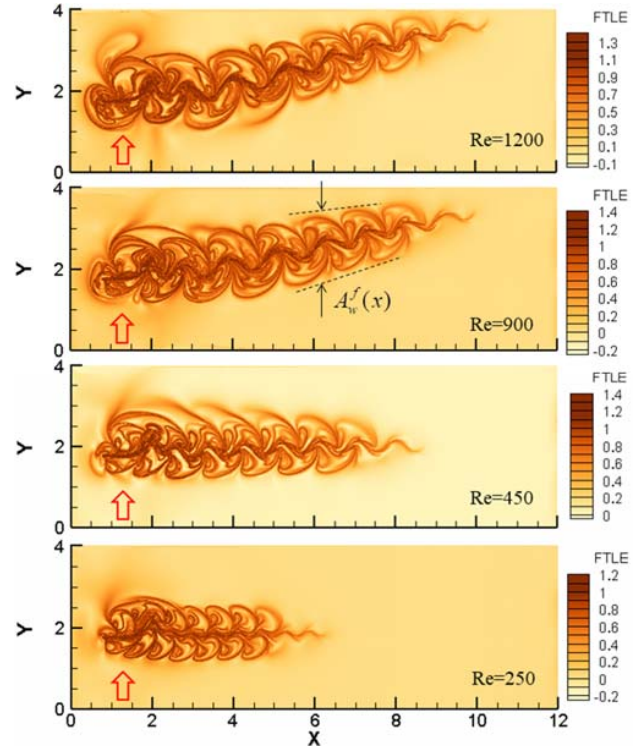

Fig. 10 Repelling LCS (stable manifolds) via forward LCS computations at $t = 0\,s$, at different Reynolds number

To have a complete picture of the LCS pattern in the flow field and also to observe evolution of these hidden structures in term of time, attracting and repelling LCS at t = 2 s are shown in Figs. 11 and 12, respectively. Red vertical arrows indicate advancement of the swimmer at t = 2 s. In contrast to all Eulerian vortex detection schemes, attracting LCS can precisely define boundary of vortices or vortical systems including several interacting vortices, as stated earlier. By comparing Figs. 9 and 11, temporal evolution of the attracting LCS is clearly visible. As one can see, by increasing viscosity, i.e., decreasing *Re* number to a low value like 250, attracting LCS identities are getting more condensed together. Fig. 12 shows anatomy of the repelling LCS at t = 2 s. As it is visible in the figure, upstream repelling hidden structures are captured, albeit its length is shorter compared to the one extracted at Fig. 10. In addition, by forward integration in this case, downstream repelling LCS is also captured. All upstream and downstream long-lived hidden LCS identities are present at all instants of time, which form the so-called 'flow skeleton'

and play an important and crucial role in the time-dependent locomotive dynamics of the nematode.
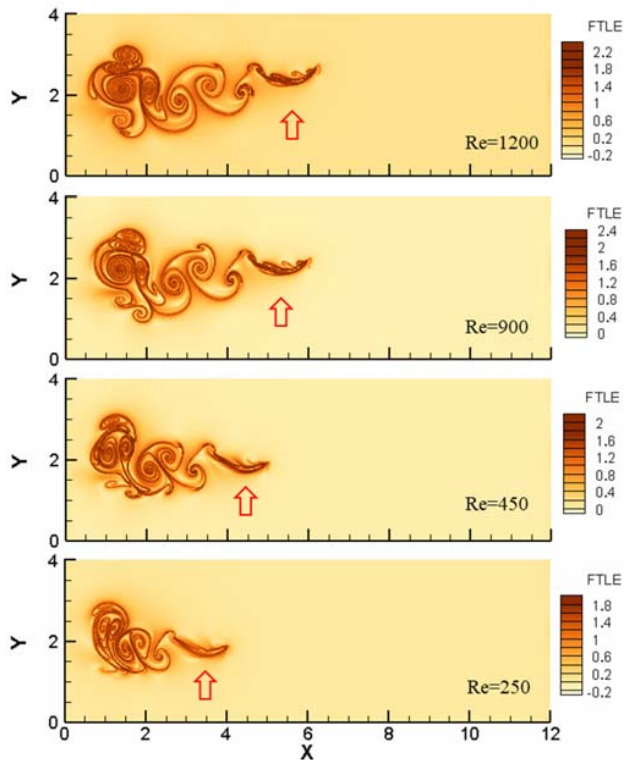

Fig. 11 Attracting LCS (unstable manifolds) via backward LCS computations at $t = 2\,s$, at different Reynolds number

VI. Conclusion

In this paper, convective flow barriers, namely LCS, as important hidden flow structures formed in the propulsive von-Kármán vortex street behind a self-propelled swimming nematode, namely *C. elegans*, were studied. In this regard, both repelling and attracting LCS were extracted at different instants of time. All simulations were performed using *IB2D* code; a computational code based on an IBM-FSI strategy. Results showed that the strategy is fully capable to simulate nematode's locomotive swimming, including: formation of the vortices due to the sequential deflections of the nematode's body and formation of Kármán vortex street in the flow field. The results also depicted that trajectory of the ejected vortices, pattern and topology of LCS identities behind the animal are majorly affected by *Re*. It was also shown that increasing of the grid resolution helps to sharply capture LCS with clear thin lines, albeit up to a certain limit. Increasing of the 'integration time' also leads to emerging of more structures identified in the flow domain. Results also showed that interactions of vortices inside the convected vortex pairs (having counter-rotating circulation) in the attracting LCS, leads to the formation of so-called '*mushroom-shaped*' structures. In addition, repelling LCS analysis exhibits formation of a semi-sinusoidal centerline curve having a sequence of closed arcs attached to it at the upstream zone of a swimming *C. elegans*. Inclined angle of the upstream oscillatory centerline curve, like the swimming path, depends on the Reynolds number. Presence of these upstream flow hidden structures defines the fluid flow portion interacting with the self-propelled animal. This portion can be also viewed as a fraction of the quiescent flow field that is disturbed by the swimming process of the animal versus time, which can be adopted by potential predators to find them within the flow field with the potential hydro-dynamical sensory capabilities of the predators [36].
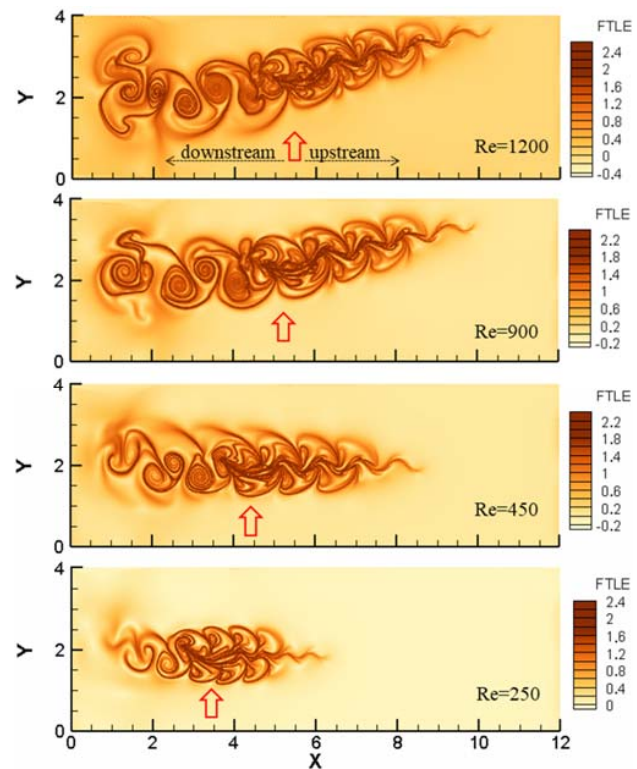

Fig. 12 Repelling LCS (stable manifolds) via forward LCS computations at $t = 2\,s$, at different Reynolds number

References

[1] A. Taheri, *Fluid Dynamics and Bio-Propulsion of Animal Swimming in Nature (Bionics)*. 1st ed., Tehran: Arshadan Publication, 20 Chapters, 692 pages, 2021.

[2] M.S.U. Khalid, J. Wang, I. Akhtare, H. Dong, M. Liu, A. Hemmati, "Why do anguilliform swimmers perform undulation with wavelengths shorter than their bodylengths?", *Physics of Fluids*, vol.33, no.3, 031911, DOI:10.1063/5.0040473, 2021.

[3] A.P. Maertens, A. Gao and M.S. Triantafyllou, "Optimal undulatory swimming for a single fish-like body and for a pair of interacting swimmers", *Journal of Fluid Mechanics*, vol.813, pp.301-345, 2017.

[4] N. Li, H. Liu, Y. Su, "Numerical study on the hydrodynamics of thunniform bio-inspired swimming under self-propulsion", *PLoS ONE*, vol.12, no.3, 2017.

[5] K.N. Lucas, N. Johnson,W.T. Beaulieu, E. Cathcart, G. Tirrell, S.P. Colin, B.J. Gemmell, J.O. Dabiri, and J.H. Costello, "Bending rules for animal propulsion", *Journal of Nature Communications*, vol.5, no.3293, , pp.1-7, DOI: 10.1038/ncomms4293, 2014.

[6] A. Taheri, "Lagrangian coherent structure analysis of jellyfish swimming using immersed boundary FSI simulations", *Journal of Mechanical and Civil Engineering*, vol.15, no.1, pp.69-74, 2018.

[7] J.G. Miles and N.A. Battista, "Naut your everyday jellyfish model: exploring how tentacles and oral arms impact locomotion", *Fluids*, vol.4, no.169, doi:10.3390/fluids4030169, 2019.

[8] A. Taheri, "Hydrodynamic impacts of prominent longitudinal ridges on the 'whale shark' swimming", *Research in Zoology*, 2020, vol.10, no.1, pp.18-30, 2020.

[9] K. Bang, J. Kim, S.I. Lee and H. Choi, "Hydrodynamic role of longitudinal dorsal ridges in a leatherback turtle swimming", Scientific Reports, *Nature Journal*, vol.6, no. 34283, doi:10.1038/srep34283, 2016

[10] A. Taheri, "On the hydrodynamic effects of humpback whale's ventral pleats", *American Journal of Fluid Dynamics*, vol.8, no.2, pp.47-62, 2018.

[11] A. Taheri, "A meta-model for tubercle design of wing planforms inspired by humpback whale flippers", *International Journal of Aerospace and Mechanical Engineering*, vol.12, no.3, pp.315-328, 2018.

[12] Photo from Bob Goldstein Lab, Department of Biology, *University of North Carolina* at Chapel Hill.

[13] B. Weischer and D.J F. Brown, *An Introduction to Nematodes: General Nematology: Student's Textbook*. Sofia: Pensoft Publication, 183 pages, 2000.

[14] R. Ghosh and S.W. Emmons, "Episodic swimming behavior in the nematode *C. elegans*", *Journal of Experimental Biology,* vol.211, pp. 3703-3711, 2008.

[15] J. Sznitman, X. Shen, R. Sznitman and P.E. Arratia, "Propulsive force measurements and flow behavior of undulatory swimmers at low Reynolds number", *Physics Of Fluids*, vol.22, no.121901, 2010.

[16] K.T. Du Clos, J.O. Dabiri, John H. Costello, S.P. Colin, J.R. Morgan, S.M. Fogerson and B.J. Gemmell, "Thrust generation during steady swimming and acceleration from rest in anguilliform swimmers", *Journal of Experimental Biology*, vol.222, jeb212464. doi: 10.1242 /jeb. 212464, 2019.

[17] J.S. Park, D. Kim, J.H. Shina and D.A. Weitz, "Efficient nematode swimming in a shear thinning colloidal suspension", *Soft Matter Journal -Royal Society of Chemistry*, doi: 10.1039/c5sm01824b, 2015.

[18] E.D. Tytella, C.Y. Hsub, T.L. Williamsc, A.H. Cohena and L.J. Faucib, "Interactions between internal forces, body stiffness, and fluid environment in a neuromechanical model of lamprey swimming", *PNAS Journal*, vol.107, no.46, pp.19832–19837, 2010.

[19] C. S. Peskin, "The immersed boundary method", *Acta Numerica Journal*, vol.11, pp.479-517, 2002.

[20] I. Borazjani, 'Numerical simulations of fluid-structure interaction problems in biological flows', Ph.D. thesis, Department of Mechanical Engineering*, University of Minnesota*, 2008.

[21] N.A. Battista, A.J. Baird, L.A. Miller, "A mathematical model and MATLAB code for muscle-fluid-structure simulations", *Journal of Integrative and Comparative Biology*, vol.55, no.5, pp.901-911, 2015.

[22] N.A. Battista, W.C. Strickland, and L.A. Miller, "IB2d: a Python and MATLAB implementation of the immersed boundary method", *Bioinspiration and Biomimicry Journal*, vol.12, no.3, 036003, 2017.

[23] S.C. Shadden, J.O. Dabiri, and J.E. Marsden, Lagrangian analysis of fluid transport in empirical vortex ring flows, *Journal of Physics of Fluid*, vol.18, no.047105, pp.1-11, 2006.

[24] N.A. Battista, "Fluid-Structure Interaction for the Classroom: Interpolation, Hearts, and Swimming!", *SIAM Review*, vol.63, no.1, pp. 181-207, 2021.

[25] N.A. Battista, "Swimming through parameter subspaces of a simple anguilliform swimmer", *Integrative and Comparative Biology*, vol. 60, no. 5, pp. 1221–1235, 2020.

[26] N.A. Battista, "Diving into a Simple Anguilliform Swimmer's Sensitivity", *Integrative and Comparative Biology*, vol. 60, no. 5, pp. 1236–1250, 2020.

[27] U.E. Ogunka, M. Daghooghi, A.M. Akbarzadeh and I. Borazjani, "The ground effect in anguilliform swimming", *Biomimetics Journal*, doi:10.3390/biomimetics5010009, 2020.

[28] S.K. Robinson, "Coherent motions in the turbulent boundary layer", *Journal of Fluid Mechanics*, vol.23, pp.601-639, 1991.

[29] M.A. Green, C.W. Rowley and Haller G., "Detection of Lagrangian coherent structures in three-dimensional turbulence", Journal of Fluid Mechanics, vol.572, pp.111-120, 2007.

[30] J.C.R. Hunt, A.A. Wraya and P. Moin, "Eddies, stream, and convergence zones in turbulent flows", *Center for Turbulent Research Report CTR-S88*, pp.193-208, 1988.

[31] J. Jeong and F. Hussain, "On the identification of a vortex", *Journal of Fluid Mechanics*, vol.285, pp.69-94, 1995.

[32] J. Peng, and J.O. Dabiri, Transport of inertial particles by Lagrangian coherent structures: application to predator-prey interaction in jellyfish feeding, *Journal of Fluid Mechanics*, vol.623, pp.75–84, 2009.

[33] VTK User's Guide, Kitware: www.kitware.com.

[34] D. Lipinski, B. Cardwell and K. Mohseni, "A Lagrangian analysis of a two-dimensional airfoil with vortex shedding", *Journal of Physics A: Mathematical and Theoretical*, vol.41, no.3444011, pp.1-22, 2008.

[35] J. Peng and J.O. Dabiri, "The upstream wake of swimming and flying animals and its correlation with propulsive efficiency", *Journal of Experimental Biology,* vol.211, pp.2669-2677, 2008.

[36] S.P. Colin, J.H. Costello, L.J. Hansson, J. Titelman and J.O. Dabiri, "Stealth predation and the predatory success of the invasive Ctenophre *Mnemiopsis leidyi*", *PNAS Journal*, doi: 10.1073/pnas.100 3170107, pp.1-5, 2010.